Proceedings of the Joint Austrian Computer Vision and Robotics Workshop 2020 DOI: 10.3217/978-3-85125-752-6-15

Several Approaches for the Optimization of Arm Motions of Humanoids

Daniel Lichtenecker, Gabriel Krög, Hubert Gattringer and Andreas Müller
Institute of Robotics, Johannes Kepler University Linz,
Altenbergerstraße 69, 4040 Linz, Austria
www.robotik.jku.at
{daniel.lichtenecker,gabriel.kroeg,hubert.gattringer,a.mueller}@jku.at

Abstract. *This paper presents several point-to-point optimization tasks of humanoid arm motions. The focus lies on optimization of elementary arm motions. Several cost functions for optimization tasks are defined. Tasks in respect of time optimal control, minimizing joint loads and maximizing the vertical torque of the torso are presented. The dynamic optimal control problem is transformed into a static parametric optimization problem by using B-spline curves. The optimization is carried out with the Sequential Quadratic Programming algorithm.*

1. Introduction

In general, robotic systems as humanoids are complex structures which are able to interact with their environment. The research on humanoid robots is a major and challenging part in the field of robotics. Various humanoid robotic systems have been developed in the past, see e.g. [5, 7]. Moreover, a humanoid walking machine is developed at the Johannes Kepler University Linz [6]. Fig. 1 shows the modular setup of the humanoid by means of submodules. In this configuration, the system possesses of 6 degrees of freedom (DOFs) per leg and 1 DOF per arm.

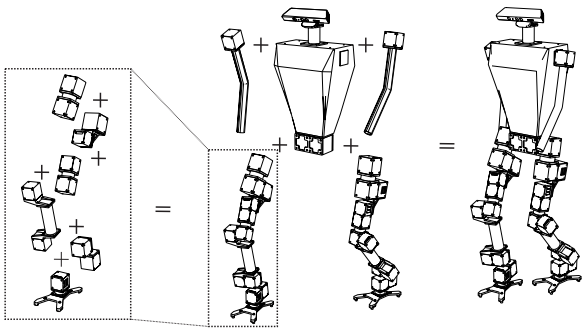

Figure 1: Schematic representation of the biped

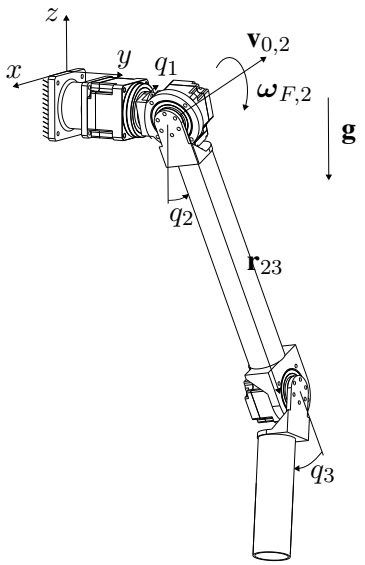

Figure 2: Schematic representation of the analyzed arm system

Especially the arm plays an important role regarding interaction or manipulation of an object. Moreover, arms are used to counterbalance the torque about the vertical axis. In order to achieve a higher degree of mobility of the arm submodule, a new arm system is developed. The system consists of 3 actuators and structural elements which are modeled as rigid bodies. The shoulder is represented by 2 DOFs and the elbow has 1 DOF. That setup is an approach toward the 7 DOFs arm module as presented in [1]. In this paper the arm module shown in Fig. 2 is considered (which will replace the rigid arm in Fig. 1). The paper focuses on optimization of elementary arm motions with respect to various goals. Start and final configurations of the arm system will be regarded as known from the human gait. As shown in Fig. 2, the arm system is spatial fixed for all further investiga-

tions.

2. Dynamic Modeling

In general, a multibody model describes the full dynamical behavior of a system. The equations of motion can be developed by the Projection Equation [2]. This method is efficient to derive the dynamic of recurrent subsystems. A typical subsystem in robotics consists of structural elements and actuators.

2.1. Subsystem Modeling

As already mentioned, modeling by means of subsystems is useful for robotic systems. Moreover, constraint forces and torques $\mathbf{Q}^c$ for coupling subsystems can be determined without additionally effort. The Projection Equation in subsystem representation is given by

$$\sum_{n=1}^{N_{sub}} \left(\frac{\partial \dot{\mathbf{y}}_n}{\partial \dot{\mathbf{q}}} \right)^\top \underbrace{\{\mathbf{M}_n \ddot{\mathbf{y}}_n + \mathbf{G}_n \dot{\mathbf{y}}_n - \mathbf{Q}_n\}}_{\mathbf{Q}_n^c} = \mathbf{0}, \quad (1)$$

$$\mathbf{Q}_n^c = \sum_{i=1}^{N_n} \left[\left(\frac{\partial \mathbf{v}_c}{\partial \dot{\mathbf{y}}_n} \right)^\top \left(\frac{\partial \boldsymbol{\omega}_c}{\partial \dot{\mathbf{y}}_n} \right)^\top \right]_i \times \begin{bmatrix} \dot{\mathbf{p}} + \tilde{\boldsymbol{\omega}}_R \, \mathbf{p} - \mathbf{f}^e \\ \dot{\mathbf{L}} + \tilde{\boldsymbol{\omega}_R} \, \mathbf{L} - \mathbf{M}^e \end{bmatrix}_i \quad (2)$$

with N_{sub} subsystems and N_n bodies. The absolute velocity of the center of mass and the angular velocity of the i-th body are represented by $\mathbf{v}_{c,i} \in \mathbb{R}^3$ and $\boldsymbol{\omega}_{c,i} \in \mathbb{R}^3$, $\boldsymbol{\omega}_{R,i} \in \mathbb{R}^3$ is the angular velocity of a chosen body fixed reference frame. The vector of linear momentum and the vector of angular momentum are given by $\mathbf{p}_i = m_i \mathbf{v}_{c,i}$ and $\mathbf{L}_i = \mathbf{J}_i^c \boldsymbol{\omega}_{c,i}$. Mass and inertia tensor are denoted m_i and $\mathbf{J}_i^c \in \mathbb{R}^{3,3}$, respectively. Impressed forces and torques are given by $\mathbf{f}_i^e \in \mathbb{R}^3$ and $\mathbf{M}_i^e \in \mathbb{R}^3$. The vector $\mathbf{q} \in \mathbb{R}^N$ represent the N minimal coordinates of the system. The describing velocities of each subsystem are given by

$$\dot{\mathbf{y}}_n = \left(\mathbf{v}_0^\top \; \boldsymbol{\omega}_F^\top \; \dot{q} \right)_n^\top \in \mathbb{R}^7, \quad (3)$$

where $\mathbf{v}_{0,n}$ is the translational velocity of the coupling point, $\boldsymbol{\omega}_{F,n}$ is the guidance rotational velocity and $\dot{q}$ is the relative joint velocity of the n-th subsystem. In this paper, the 3 rotational coordinates $\mathbf{q} = (q_1 \; q_2 \; q_3)^\top$ are introduced as DOFs. Moreover, 3 subsystems are considered to derive the equations of motion. The describing velocities of the second subsystem can be seen in Fig. 2.

2.2. Joint Forces and Torques

As shown by 2.1, the occurring reaction forces and torques of the n-th subsystem can be determined by

$$\mathbf{Q}_n^c = \mathbf{M}_n \ddot{\mathbf{y}}_n + \mathbf{G}_n \dot{\mathbf{y}}_n - \mathbf{Q}_n, \quad (4)$$

with the mass matrix of the subsystem $\mathbf{M}_n \in \mathbb{R}^{7,7}$, the matrix of centrifugal and Coriolis forces $\mathbf{G}_n \in \mathbb{R}^{7,7}$ and the vector of forces on the subsystem $\mathbf{Q}_n \in \mathbb{R}^7$. Without projection into minimal coordinates, joint forces and torques regarding the three subsystems are given by

$$\begin{pmatrix} {}_1\mathbf{Q}^c \\ {}_2\mathbf{Q}^c \\ {}_3\mathbf{Q}^c \end{pmatrix} = \begin{bmatrix} \mathbf{E} & \mathbf{T}_{21}^\top & \mathbf{T}_{31}^\top \\ \mathbf{0} & \mathbf{E} & \mathbf{T}_{32}^\top \\ \mathbf{0} & \mathbf{0} & \mathbf{E} \end{bmatrix} \begin{pmatrix} \mathbf{Q}_1^c \\ \mathbf{Q}_2^c \\ \mathbf{Q}_3^c \end{pmatrix}. \quad (5)$$

The matrix

$$\mathbf{T}_{np} = \begin{pmatrix} \mathbf{R}_{np} & \mathbf{R}_{np} \, {}_p\tilde{\mathbf{r}}_{pn}^\top & \mathbf{R}_{np} \, {}_p\tilde{\mathbf{r}}_{pn}^\top \mathbf{e}_D \\ \mathbf{0} & \mathbf{R}_{np} & \mathbf{R}_{np} \mathbf{e}_D \\ \mathbf{0} & \mathbf{0} & \mathbf{0} \end{pmatrix} \quad (6)$$

maps a quantity from the predecessor frame p into the frame of interest n. $\mathbf{R}_{np} \in \mathbb{R}^{3,3}$ is the rotation matrix to transform coordinate vectors resolved in the frame p into frame n, ${}_p\mathbf{r}_{pn} \in \mathbb{R}^3$ is the displacement vector from the coupling point at the predecessor frame p to that on frame n and the vector $\mathbf{e}_D \in \mathbb{R}^3$ is the axis of rotation. The transformation matrix is a result of the kinematical chain [4].

3. Problem Definition

This section reports on different optimization tasks for point-to-point (PTP) trajectory planning. In this paper, the optimal dynamic motion problem is transformed into a static parametric optimization problem. The joint trajectories are represented by B-spline curves parameterized by a set of control points $\mathbf{d} = (d_{1,1} \; \cdots \; d_{1,n} \; d_{2,1} \; \cdots \; d_{2,n} \; d_{3,1} \; \cdots \; d_{3,n})^\top$, i.e. $\mathbf{q} = \mathbf{q}(\mathbf{d})$ and thus $\dot{\mathbf{q}} = \dot{\mathbf{q}}(\mathbf{d})$ and $\ddot{\mathbf{q}} = \ddot{\mathbf{q}}(\mathbf{d})$. For practical applications, several physical restrictions of the robotic system have to be considered. In this paper, constraints regarding to initial and final state, minimal and maximal joint angles as well as maximal motor velocities and torques are regarded. The mathematical formulation of the constraints are given in Eq. (8)–(14). The task of trajectory optimization leads to a non-linear optimization problem (NLP). Different cost functions are presented in the following.

3.1. Time Optimal Control

The optimization problem for time optimal control is defined as

$$\min_{t_f,\mathbf{d}} \int_0^{t_f} 1dt \tag{7}$$

s.t.

$$\mathbf{q}(0,\mathbf{d}) = \mathbf{q}_0 \tag{8}$$

$$\mathbf{q}(t_f,\mathbf{d}) = \mathbf{q}_{t_f} \tag{9}$$

$$\dot{\mathbf{q}}(0,\mathbf{d}) = \mathbf{0} \tag{10}$$

$$\dot{\mathbf{q}}(t_f,\mathbf{d}) = \mathbf{0} \tag{11}$$

$$\mathbf{q}_{\text{min}} \leq \mathbf{q}(\mathbf{d}) \leq \mathbf{q}_{\text{max}} \tag{12}$$

$$-\dot{\mathbf{q}}_{\text{max}} \leq \dot{\mathbf{q}}(\mathbf{d}) \leq \dot{\mathbf{q}}_{\text{max}} \tag{13}$$

$$-\mathbf{Q}_{\text{max}} \leq \mathbf{Q}(\mathbf{d}) \leq \mathbf{Q}_{\text{max}} \tag{14}$$

$$\mathbf{Q}(\mathbf{q}(\mathbf{d})) = \mathbf{M}(\mathbf{q}(\mathbf{d}))\ddot{\mathbf{q}}(\mathbf{d}) + \mathbf{g}(\mathbf{q}(\mathbf{d}),\dot{\mathbf{q}}(\mathbf{d})). \tag{15}$$

In this case, the final time t_f and the set of control points $\mathbf{d}$ to parameterize the B-splines are regarded as optimization variables. Eq. (15) represents the dynamical behavior of the robotic system in minimal representation. $\mathbf{M} \in \mathbb{R}^{3,3}$ is the global mass matrix, $\mathbf{g} \in \mathbb{R}^3$ includes non-linear terms and $\mathbf{Q} \in \mathbb{R}^3$ is the global vector of generalized forces. The restrictions in Eq. (8)–(12) are associated to process requirements and those in Eq. (13)–(14) are defined by chosen motors. This equality and inequality constraints were used for all optimization tasks in the following.

3.2. Minimizing Joint Loads

Aim of this optimization task is to minimize dynamic joint forces and torques between ground/torso and arm of the humanoid walking machine. The final time t_f for the motion is predefined in this task. The cost function is given by

$$\min_{\mathbf{d}} {}_1\mathbf{Q}^{c\top}\,{}_1\mathbf{Q}^{c}. \tag{16}$$

The set of control points $\mathbf{d}$ are regarded as optimization variables. As mentioned above, the optimization constraints are given by Eq. (8)–(14). Note, the occurring joint forces and torques can be calculated with Eq. (5).

3.3. Maximizing the Vertical Torque of the Torso

During gait, arms are used to counterbalance the torque around the vertical axis. A momentum control approach with this quantity is presented in [6]. Hence, another optimization strategy is to find a proper set of control points $\mathbf{d}$ such that the cost function

$$\max_{\mathbf{d}} {}_1Q_6^{c\top}\,{}_1Q_6^{c} \tag{17}$$

is maximized. Once again, optimization constraints are given by Eq. (8)–(14). The quantity ${}_1Q_6^c$ is the sixth entry of ${}_1\mathbf{Q}^c$ and describes the joint torque of the first subsystem in the opposite direction of the gravity vector.

4. Optimization Method

The Sequential Quadratic Programming (SQP) algorithm was chosen to solve all considered optimization problems. This approach is also used in [3] for trajectory planning. The SQP method requires an valid initial guess for trajectories. In this case, the initial trajectories are defined as B-splines. Properties of B-splines can be found in [8]. An initial guess for the arm angels $\mathbf{q}$ are found by interpolating the initial and final position as well as some support points with a B-spline of degree 4. Furthermore, velocities and accelerations at the initial and final position are set to zero. Twenty control points were chosen to initialize each of the three polynomials. Fig. 3 shows exemplary an initial guess trajectory.

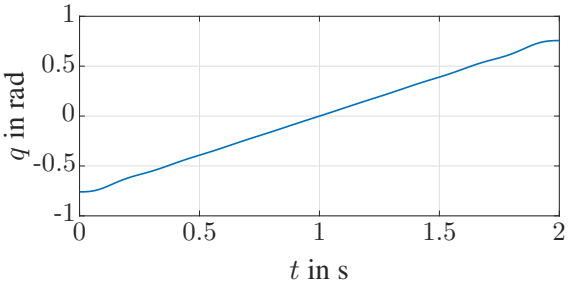

Figure 3: Example of an initial guess trajectory

5. Simulation Results

In this section, relevant results of the optimization tasks are presented. The typical arm motion during a step of the biped is defined by the start configuration $\mathbf{q}_0 = \left(-\frac{\pi}{4}\,0\,0\right)^\top \text{rad}$ and the final configuration $\mathbf{q}_{t_f} = \left(\frac{\pi}{4}\,0\,\frac{\pi}{4}\right)^\top \text{rad}$ of the minimal coordinates. Moreover, limits regarding joint angles are defined by $\mathbf{q}_{\text{min}} = \left(-\frac{\pi}{2}\,0\,0\right)^\top \text{rad}$ and $\mathbf{q}_{\text{max}} = \left(\pi\;\pi\;\frac{3\pi}{4}\right)^\top \text{rad}$. Maximal motor rotational velocities and torques are given by $\dot{\mathbf{q}}_{\text{max}} = (12.6\;6.3\;12.6)^\top\,\text{rads}^{-1}$ and $\mathbf{Q}_{\text{max}} = (415\;480\;165)^\top\,\text{N m}$. Note, that all motor torques

and rotational velocities of the following figures are normalized w.r.t. their physical limits.

5.1. Time Optimal Control

Fig. 4 shows the normalized motor torques and rotational velocities of time optimal control problem. For time optimal optimization tasks, it is obvious that at least one motor restriction is active. The final time is given by $t_f = 0.83\,\mathrm{s}$. Moreover, all physical limits of the motors are well considered. Occurring joint forces and torques of the first subsystem are shown in Fig. 5.

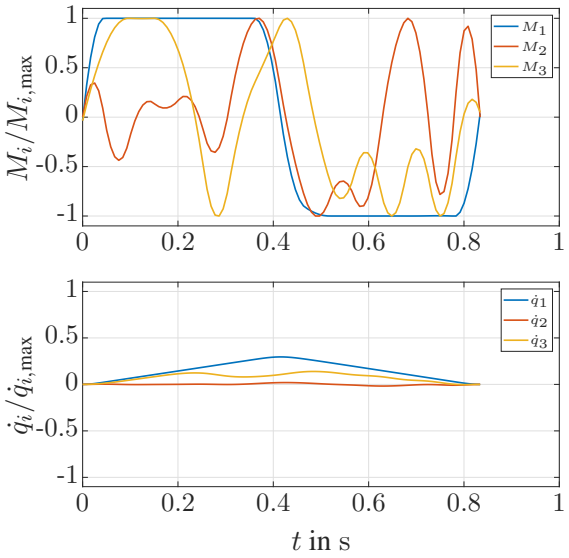

Figure 4: Normalized motor torques and rotational velocities of the time optimal control

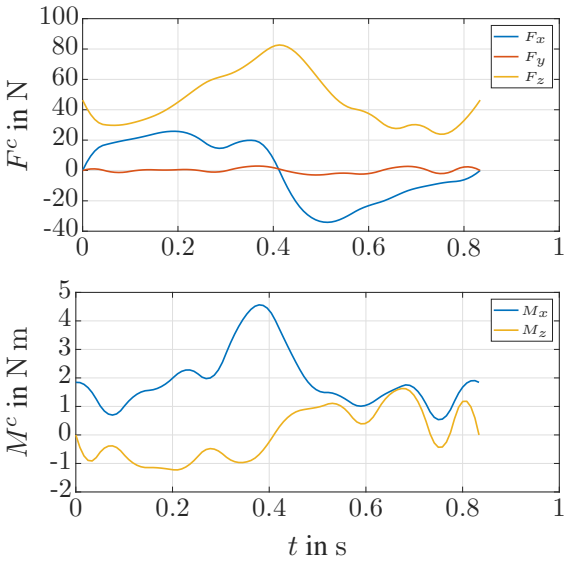

Figure 5: Joint forces and torques of the time optimal control

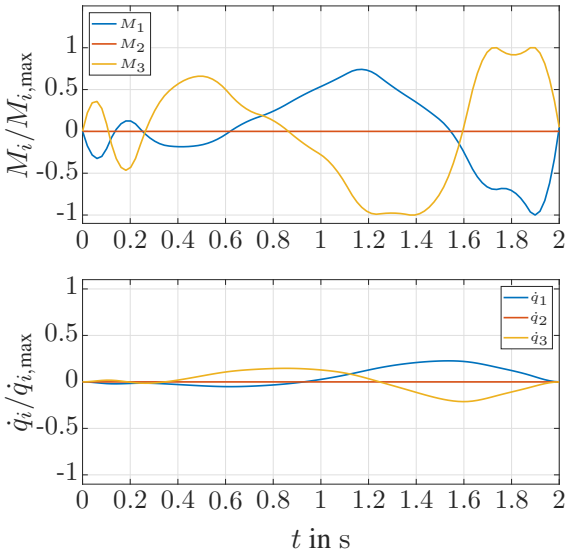

Figure 6: Normalized motor torques and rotational velocities of the joint load minimization

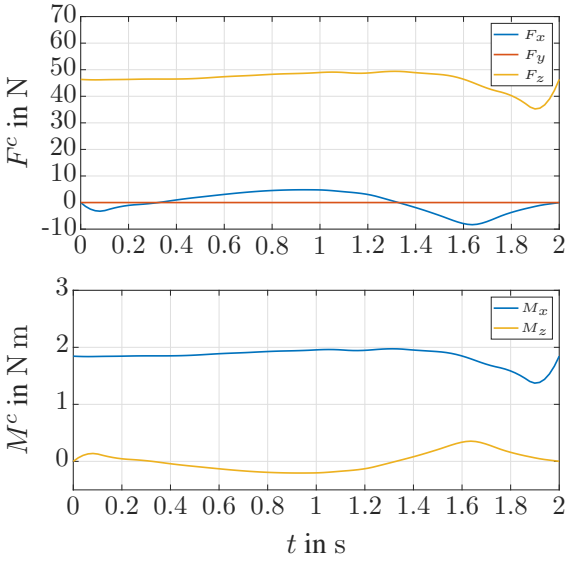

Figure 7: Joint forces and torques of the joint load minimization

5.2. Minimizing Joint Loads

In comparison to time optimal control, the final time $t_f = 2\,\mathrm{s}$ of this optimal control is predefined due to the walking speed of the analyzed biped. Fig. 6 and Fig. 7 shows the dynamical behavior of this task. Motor restrictions are almost inactive and the occurring joint forces and torques are reduced in comparison to Fig. 5.

5.3. Maximizing the Vertical Torque of the Torso

As to the last subsection 5.2, the final time $t_f = 2\,\mathrm{s}$ is also predefined in this task. Optimization re-

sults of the maximization task are shown in the following figures. Almost all motor torque restrictions are active due to the maximization. As can be seen in Fig. 8, the first arm moves at the start in the negative direction. The resulting motion performs as a swing-up procedure.

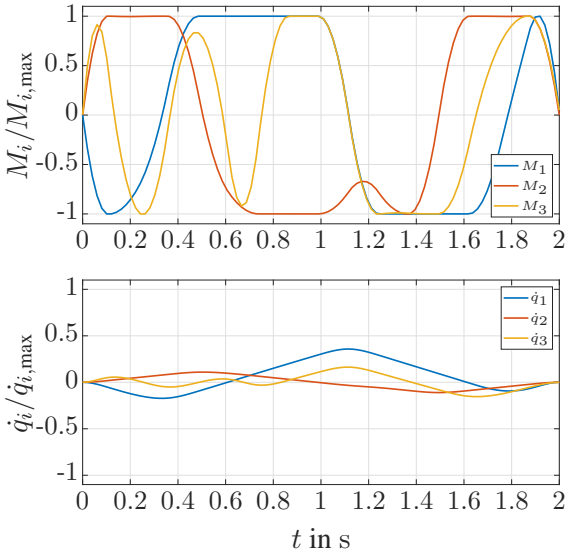

Figure 8: Normalized motor torques and rotational velocities of the vertical torque maximization

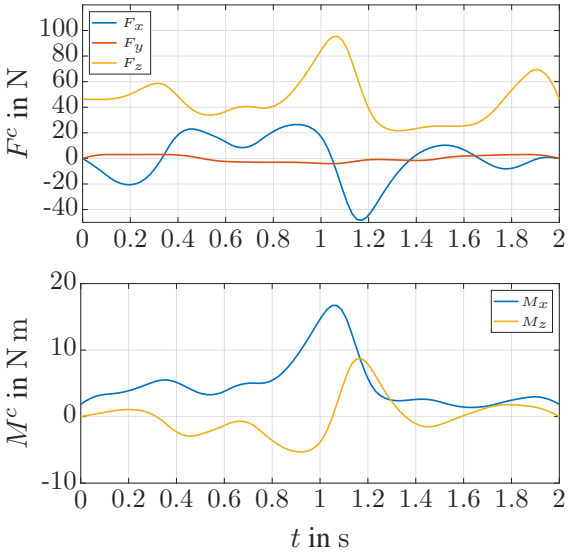

Figure 9: Joint forces and torques of the vertical torque maximization

6. Conclusion

Arm systems of humanoids are used in different ways, e.g. to counterbalance the torque around the vertical axis. Motion planning in relation to various tasks becomes an important role. Therefore, in this paper different optimization goals regarding arm motions were analyzed. Cost functions with respect to time optimal control, joint load minimization and vertical torque maximization were considered. The dynamic optimization process has been converted into a static optimization process by using B-splines curves to formulate trajectories. The NLP were solved with the SQP method.

Acknowledgments

This work has been partially supported by the "LCM – K2 Center for Symbiotic Mechatronics" within the framework of the Austrian COMET-K2 program. Additional support is provided by the Linz Institute of Technology.

References

[1] M. Benati, S. Gaglio, P. Morasso, V. Tagliasco, and R. Zaccaria. Anthropomorphic robotics. *I. Representing Mechanical Complexity*, pages 125–140, 180.

[2] H. Bremer. *Elastic Multibody Dynamics: A Direct Ritz Approach*. Springer Verlag, 2008.

[3] T. Chettibi, H. Lehtihet, M. Haddad, and S. Hanchi. Minimum cost trajectory planning for industrial robots. *European Journal of Mechanics - A/Solids*, 23(4):703 – 715, 2004.

[4] H. Gattringer. *Starr-elastische Robotersysteme: Theorie und Anwendungen*. Springer Verlag, 2011.

[5] K. Hirai, M. Hirose, Y. Haikawa, and T. Takenaka. The development of honda humanoid robot. In *Proceedings. 1998 IEEE International Conference on Robotics and Automation*, volume 2, pages 1321–1326, 1998.

[6] J. Mayr. *Development and Control of a Modular Bipedal Walking Robot*. Trauner Verlag, 2016.

[7] G. Nelson, A. Saunders, N. Neville, B. Swilling, J. Bondaryk, D. Billings, C. Lee, R. Playter, and M. Raibert. Petman: A humanoid robot for testing chemical protective clothing. *Journal of the Robotics Society of Japan*, 30(4):372–377, 2012.

[8] L. Piegl and W. Tiller. *The NURBS Book*. Springer Verlag, 1997.